Journal of Cereal Science 105 (2022) 103470

Contents lists available at ScienceDirect

Journal of Cereal Science

journal homepage: www.elsevier.com/locate/jcs

Localisation of iron and zinc in grain of biofortified wheat

Yongfang Wan [a], Theodora Stewart [b], Maral Amrahli [b], Jessica Evans [c], Paul Sharp [d], Velu Govindan [e], Malcolm J. Hawkesford [a], Peter R. Shewry [a,*]

[a] Plant Science, Rothamsted Research, Harpenden, UK
[b] London Metallomics Facility, Kings College, London, UK
[c] Computational and Analytical Sciences, Rothamsted Research, Harpenden, UK
[d] Nutritional Sciences, Kings College, London, UK
[e] International Maize and Wheat Improvement Center (CIMMYT), Texcoco, Mexico

ARTICLE INFO

Keywords:
Wheat grain
Biofortification
Micronutrients
LA-ICP-MS
Localisation
Zinc
Iron

ABSTRACT

The dietary contributions of iron (Fe) and zinc (Zn) from cereals are determined by concentrations, locations and chemical forms. A genetically biofortified wheat line showed higher concentrations of Zn and Fe than three control lines when grown over two years. The mineral distributions determined using imaging (histochemical staining and LA-ICP-MS), sequential pearling and hand dissection showed no consistent differences between the two lines. Fe was most abundant in the aleurone layer and the scutellum and Zn in the scutellar epithelium, the endosperm transfer cells and embryonic axis. Pearling fractions showed positive correlations between the concentration of P and those of Zn and Fe in all fractions except the outermost layer. This is consistent with Fe and Zn being concentrated in phytates. Developing grains showed decreasing gradients in concentration from the proximal to the distal ends. The concentrations of Fe and Zn were therefore higher in the biofortified line than the control lines but their locations did not differ.

1. Introduction

Wheat is produced on a greater area and grown over a wider geographical range than any other arable crop. It accounts for over a quarter of all cereal production and is particularly dominant in temperate countries where it accounts for between about 10% and over 50% of total calories consumed. However, although wheat is widely viewed a source of energy in the diet, it also contributes a range of other components which are essential for nutrition and health, including mineral micronutrients. For example, bread contributes 10–13% of the energy in the UK diet and 15–17% and 11–13% of the daily intakes of iron (Fe) and zinc (Zn), respectively (Bates et al., 2014a,b). These contributions are important because deficiencies of Fe and Zn are estimated to affect about 2 million people globally. WHO have estimated that 43% of children and 29% of women of reproductive age globally have anaemia, half of which results from Fe deficiency (WHO, 2015), while Zn deficiency is estimated to affect about 155 million children globally (WHO, 2013). Although micronutrient deficiencies are most widespread in developing countries they also occur in the developed world. For example, Fe intakes substantially below the lower reference levels have been reported for young children (1.5–3.5 years), girls (11–18) and women (19–49) in the UK (SACN, 2010).

The importance of wheat as a source of mineral micronutrients has led to many studies aimed at increasing the concentrations of Fe and Zn in commercially grown genotypes. These have shown variation in the concentrations of both minerals, for example, Zhao et al. (2009) reported ranges from 28.8 mg to 37.6 mg Fe/kg dry wt. and 13.5 mg–20.8 mg Zn/kg dry wt. in 150 bread wheat genotypes grown on a single site. However, this variation has proved difficult to exploit, due to strong effects of environment and generally low heritability. Nevertheless, Velu et al. (2018) reported a genome-wide association study (GWAS) of 330 lines of bread wheat, identifying two major quantitative trait locus (QTL) regions for Zn concentration which were exploited to develop Zn-biofortified wheat lines which are currently being evaluated in human feeding trials (Lowe et al., 2020).

The effectiveness of wheat as a source of minerals is not only determined by their total concentrations but also by their bioavailability, which is in turn determined by their location and chemical speciation. Both Fe and Zn are known to be concentrated in the aleurone layer and embryo of the mature grain and are present at only low levels

* Corresponding author.
E-mail address: peter.shewry@rothamsted.ac.uk (P.R. Shewry).

https://doi.org/10.1016/j.jcs.2022.103470
Received 6 January 2022; Received in revised form 24 March 2022; Accepted 25 March 2022
Available online 3 April 2022

in the starchy endosperm (white flour) which is most widely consumed (reviewed by Balk et al., 2018). Furthermore, the minerals within these tissues are largely present in discrete bodies (phytin globoids) as complexes with phytic acid (inositol hexakisphosphate) (Neal et al., 2013). Phytic acid has a cyclic structure with six phosphate groups, which bind metal ions, and the resulting phytates have low solubility which limits the bioavailability of the minerals. In the case of wheat, the bioavailability of Zn and Fe in wholegrain has been estimated at about 25% and 10% of the total, respectively (Bouis and Welch, 2010).

The objective of the present study was therefore to determine whether there are differences in the locations of minerals within the grains of biofortified and conventional wheat lines, by comparing samples of a selected high Zn line (Zn1) and three control lines grown in replicated field trials over two years.

2. Experiments

2.1. Grain samples

One high Zn line (Zinc-Shakti), and three control lines (MAYIL#2, KACHU#1, and BAJ#1) of bread wheat (*Triticum aestivum* L.) were selected for comparison. Zinc-Shakti (Croc_1/Ae.squarrosa(210)//Inqalab91*2/Kukuna/3/PBW343*2/Kukuna) (Zn1) has about 20–40% higher concentrations of Fe and Zn, respectively, than local varieties. It was developed at CIMMYT, Mexico, using synthetic hexaploid derivatives from the tetraploid *T. durum* and diploid *Ae. tauschii*. Kachu #1 (Con2) is a high-yielding CIMMYT wheat variety which was released in India as DPW-621-50 but has low grain Fe and Zn concentrations. QTL mapping analysis using Kachu x Zinc-Shakti revealed that high Zn and Fe alleles were contributed from the synthetic hexaploid parent which was derived from *T. durum* × *Ae. tauschii* (Rathan et al., 2021). Baj#1 (Con3) is a commercial check developed at CIMMYT with normal concentrations of Fe and Zn. Mayil#2 (Con1) was initially developed as a Zn biofortified line but the trait was not expressed in subsequent generations and it was therefore included in the current study as a control.

The four lines were grown in field trials (three replicates) at Rothamsted Research (Harpenden, UK) in 2018 (plot size, 1m × 1m) and 2019 (plot size, 1.8m × 4.23m). 50, 100, and 50 kg/ha of nitrogen fertilizer (as ammonium nitrate) were applied at the tillering, stem extension, and flag leaf emergence stages respectively. Plots received standard agronomic treatment for the site including applications of fungicides to prevent fungal infections. Whole caryopses were harvested at 16, 22 and 30 days after anthesis (DPA) and manually dissected into four parts as described by Shi et al. (2019). The embryo was removed and the remaining caryopsis was then divided into three approximately equal parts along the longitudinal axis (end1, end2, end3). The grain tissues were lyophilised for elemental analysis.

2.2. Pearling of grains

Samples (50g) of mature seeds grown in 2019 were pearled in a Streckel & Schrader (Hamburg, Germany) pearling mill based on the method of Tosi et al. (2011). Samples of each line were initially pearled for 1, 2, 3, 4, 5, and 10 min to construct a calibration curve which was used to calculate the times required to remove six fractions (called F1–F6) corresponding to about 4, 7, 7, 12, 10, and 10% of the grain weight. The remaining cores (about 50% of grain weight) and whole grains were milled in a centrifugal mill (Retsch, ZM200). Three biological replicates were analysed.

2.3. Histochemical staining of seeds

Developing or mature grains were cut transversely or longitudinally with a razor blade. The sections were then stained in 500 mg/L dithizone in methanol for 30 min for Zn localisation, and in 2% (w/v) potassium ferrocyanide (II) in 2% (v/v) HCI for 40 min for Fe localisation. The tissue was washed in deionized water until the background was clear and photographed using a Leica MA205 camera.

2.4. Laser ablation-inductively coupled plasma-mass spectrometry (LA-ICP-MS)

The mature grain was imbibed in water for 8 h at 4 °C, and then embedded in O.C.T compound (Tissue-Tek) at −17 °C for 2 h 30 μm thick transverse sections (across the root or leaf primordia of the embryo and centre of the endosperm) were prepared using a Cryostat (Leica CM1950), dried on poly-L-lysine adhesion slides at room temperature and checked under a microscope to determine the best sections for imaging. Elemental analysis of the grain section was carried out with an Analyte Excite 193 nm ArF*excimer-based LA system (Teledyne Photon Machines, Bozeman, MT, USA) equipped with the HelEx II two-volume ablation cell. The LA system was coupled to a Thermo Fisher Scientific iCAPTQ ICP-MS (Thermo Fisher Scientific, Waltham, MA, USA) via the Aerosol Rapid Introduction System (ARIS). Tuning of the instrument settings was performed using a NIST SRM 612 glass certified reference material (National Institute for Standards and Technology, Gaithersburg, MD,USA), optimizing for low laser-induced elemental fractionation through monitoring of $^{238}U^{+}/^{232}Th^{+}$ ratios, low oxide formation (<1%) monitoring $^{232}Th^{16}O^{+}/^{232}Th^{+}$ ratios, and high sensitivity for $^{59}Co^{+}$, $^{115}In^{+}$ and $^{238}U^{+}$. LA-ICP-MS images were acquired in a fixed dosage mode, with a vertical and horizontal spatial resolution of 10 μm. Samples were mounted inside a bespoke three slide sample holder of the HelEx II two-volume ablation cell (Teledyne Photon Machines). To correct for instrumental drift, a series of NIST 612 standard ablation scans were performed before and after each section. ICP-MS and positional data were reconstructed using the HDF-based Image Processing software (HDIP, Teledyne Photon Machines Inc., Bozeman, MT, USA). A bespoke pipeline, written in Python (version 3.8), was used to generate elemental images from reconstructed data. Negative values, attributed to instrumental noise, were replaced with zeros. Details of experimental conditions are provided in Supplementary Table S1.

2.5. Elemental analysis by ICP-OES

Samples were oven-dried at 80 °C overnight, weighed and digested using a mixture of nitric acid and perchloric acid (85:15 v/v) in open tube digestion blocks, followed by a programmed heating digestion: 60 °C for 180 min, 100 °C for 60 min, 120 °C for 60 min, 175 °C for 90 min and 50 °C until dry. The acids were removed by volatilisation and the residue dissolved in nitric acid (5% v/v). The elements were detected with Optima 7300 DV Inductively Coupled Plasma-Optical Emission Spectrometer (ICP-OES). The analyses were monitored using certified external standards and in-house standard materials. Standards and check samples were monitored and recorded using Shewhart Control Graphs and computer-based quality control packages.

2.6. Statistical methods

Statistical analyses were performed using Genstat 21 (VSN International, 2020).

The mineral concentrations of whole grain samples grown in 2018 and 2019 were analysed using analysis of variance (ANOVA). The blocking structure used was expt/rep accounting for potential variation between the two experiments (years) and the variation between the 3 blocks within each year. The treatment structure was (linetype/line) *year where linetype labels Zn1 as the treatment line and all others as control lines. This provides the following 4 tests:Linetype: test for difference between treatment and the average of the three controls.Line: test for any differences between the three controls.Linetype.year: test for change/consistency in the difference between treatment and the average of the three controls across the two years.Linetype.line.year: test for change/consistency in the differences between the three controls across

the two years.

The concentrations of Fe, Zn and P (using log transformation to satisfy the assumptions of the analysis) in pearling fractions were analysed by ANOVA using a blocking structure (replicate/plot) to account for potential variation between the replicates and the variation between plots within replicates and to ensure that differences between fractions were assessed at the within plot level. The treatment structure was (linetype/line)*fractions where linetype labels Zn1 as the treatment line and all others as control lines. This provides the following 5 tests: Linetype: test for difference between treatment and the average of the three controls.Line: test for any differences between the three controls. Fractions: test for any differences between fractions. Linetype.fractions: test for change/consistency in the difference between treatment and the average of the three controls across the fractions (or change in the difference between fractions in treatment vs control). Linetype.line.fractions: test for change/consistency in the differences between the three controls across the fractions (or change in difference between fractions across the 3 controls).

The concentrations of minerals in developing grain were analysed on the log scale to satisfy the assumptions of the analysis. Data for Fe and Zn in whole caryopses and embryos were analysed separately using ANOVA where the blocking structure block/plot accounts for variation between blocks and plots within blocks and ensure that stage comparisons are made at the within plot level.

The treatment structure (linetype/line)*stage gives the following 5 tests: Linetype: test for difference between treatment and the average of the three controls. Line: test for any differences between the three controls.Stage: test for any differences between stages. Linetype.stage: test for change/consistency in the difference between treatment and the average of the three controls across the stages (or change in the difference between stages in treatment vs control). Linetype.line.stage: test for change/consistency in the differences between the three controls across the stages (or change in difference between stages across the 3 controls).

Analyses of endosperm segments were similarly analysed using ANOVA with the blocking structure being extended to include sample stage and ensure that variation between samples from the same plot was accounted for and that the comparison of segments was made at this level. The treatment structure was also extended to include the parts and the interactions with the other terms so in addition to the test above the following tests are also given: Parts – test for differences between end1, end2 and end3. linetype.parts: test whether the difference between linetypes is different for different parts (and vice versa). stage.parts: test whether the difference between stages is different for different parts (and vice versa). linetype.line.parts: test whether the difference between control lines is different for different parts (and vice versa). linetype. stage.parts: test for a three-way interaction between linetype, stage and parts.

3. Results

3.1. Minerals in mature grain

The Zn-biofortified line Zinc-Shakthi (called Zn1) and three control lines (called Con1 to Con3) were grown in replicated field trials for two years (2018 and 2019). The concentrations (mg/kg dry wt) (Fig. 1A) and contents (μg/grain) (Supplementary Fig. S1) of Fe and Zn were determined by ICP-OES of milled whole grain (Fig. 1) and the data analysed by ANOVA (Supplementary Table S2). This showed significantly higher concentrations (mg/g dry wt.) of Zn and Fe in Zn1 than in the average of the control lines ($p < 0.001$) which were consistent across the two years ($p = 0.163$ for Fe and $p = 0.211$ for Zn). There was also evidence of differences between the three control lines for both Zn ($p = 0.028$) and Fe ($p = 0.066$) but these were not consistent across the two years ($p = 0.027$ for Zn and $p = 0.014$ for Fe). Inspection of the means and least significance difference (LSD) values showed that Zn1 differed from all three controls despite the controls being different to each other (Supplementary Table S2).

The concentration of P (also determined by ICP-OES) was also higher in Zn1 than in the mean of the control lines ($p < 0.001$), although the difference was smaller than for Fe and Zn (Fig. 1B, Supplementary Table S2). The difference between Zn1 and the mean of the controls was consistent across the two years ($p = 0.013$), but there were also differences between the three control lines ($p < 0.001$) which were not consistent across the two years ($p < 0.001$). The LSD (342.5) shows differences between the controls in 2019 (but not in 2018) with Con2 having higher P than the other controls. Zn1 was not different to Con2 in 2019 but did differ from the other two controls.

Higher contents (μg/grain) of Fe and Zn were observed in the grain of Zn1 than in the control lines (Supplementary Fig. S1, Table S2) showing that the differences in concentration were not related to grain size.

3.2. Localisation of Fe and Zn in mature grain by histochemical staining and LA-ICP-MS

Transverse sections of mature grain were prepared at three positions: at the proximal end of the grain across the root primordium (RP) and shoot primordium (RP) of the embryo and towards the distal end of the grain across the middle of the starchy endosperm (EN). These sections and longitudinal sections were stained for Zn and Fe with dithizone and

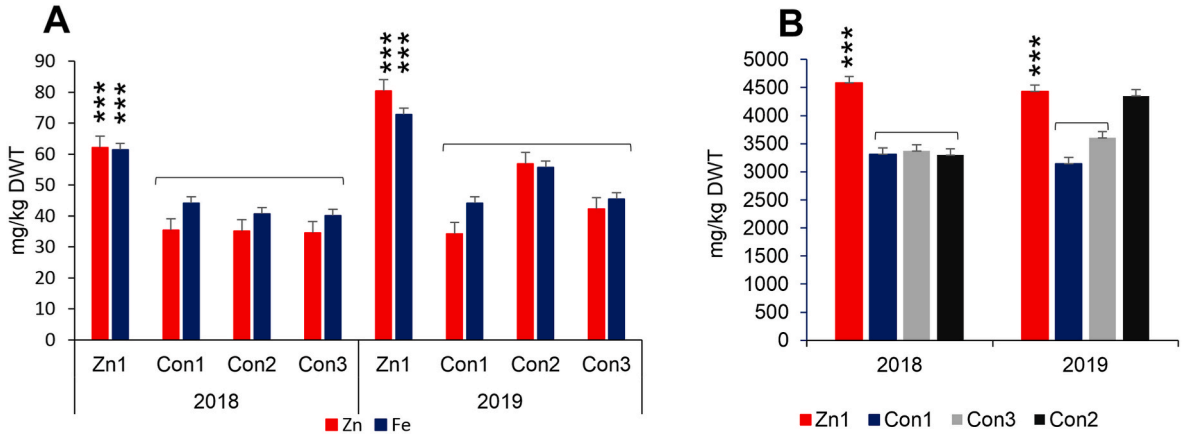

Fig. 1. The concentrations of minerals (mg/kg dry wt.) in whole grains of mature grains grown in field trials in 2017–2018 and 2018–2019. A, Zn and Fe; B, P. Error bars shown are standard errors of the means. Significant differences ($P < 0.001$) between Zn1 and the three control lines (Con1, Con2, Con3) were determined by ANOVA (Supplementary Table 2). The least significance difference (LSD) values (5%) are 11.23 and 6.58 and 342.5 for Zn, Fe and P, respectively.

Prussian blue, respectively (Fig. 2). This showed that Zn is most highly concentrated in the embryo, particularly in the leaf primordia (plumule), in the layers of cells (cortex) surrounding the pro-vasculature of the embryonic root (radicle) and in the epithelium of the scutellum. Zn is also concentrated in the aleurone cells, particularly the modified aleurone cells which form the endosperm transfer cells in the groove. By contrast, Fe is mainly concentrated in the aleurone layer, particularly in the modified aleurone and nucellar projection in the groove region, and in the scutellum (but not the embryonic axis) of the embryo. The concentration of Fe is also higher in the dorsal aleurone cells than in those surrounding the lobes. Although the embryo appeared to stain more highly for Zn in Zn1 than in the control lines, neither stain is strictly quantitative. Furthermore, the presence of background staining (which may result partly from diffusion) makes it difficult to determine whether the two minerals are also present in other tissues, particularly the starchy endosperm.

To overcome this limitation, the distributions of Zn and Fe in transverse sections of the two lines were imaged at higher resolution (10 μm) using LA-ICP-MS (Fig. 3), which allows for the simultaneous measurement of P, Fe and Zn. In contrast to staining techniques that rely on chemical reactions with specific metal species, LA-ICP-MS directly measures specific isotopes of metals providing more accurate localisation.

The LA-ICP-MS analyses essentially confirmed the results from histochemical staining, showing similar distributions of the minerals in the high and low Zn lines. The sections across the proximal part of the grain show that Fe is concentrated in the aleurone layer (particularly in the groove region) and throughout the scutellum while Zn is also present in these tissues, but is concentrated in the epithelium of the scutellum, in the shoot primordia, and cortex of the root primordium (Figs. 3 and 4). P is concentrated in the same tissues as Fe and Zn: the aleurone layer and throughout the embryo (notably the scutellum and shoot primordium). The sections across the distal starchy endosperm show that all three minerals are concentrated in the aleurone layer, with Zn and Fe (but not P) being more concentrated in the transfer cells in the groove region. Neither Fe nor Zn was detected in the starchy endosperm of the grain.

These results clearly show that Fe and Zn are localised to the same tissue regions in both the biofortified and control lines, with no evidence for significant redistribution to the starchy endosperm tissues. However, although Zn1 contained significantly higher concentrations of both Fe and Zn, neither method showed consistent differences in concentrations in the tissue sections. This may be due to technical limitations: neither stain is strictly quantitative while the quantitative accuracy of the LA-ICP-MS relies on the full removal of tissue by the laser, which can vary with differences in tissue density. To obtain fully quantifiable results, ICP-OES analysis of digested tissue fractions was carried out.

3.3. Chemical analysis of grain fractions

The distributions of Fe and Zn within the mature grain were determined by the sequential removal of fractions from the outside of the grain by pearling (Fig. 5). This was carried out with a laboratory pearling mill, removing 6 fractions. These fractions do not correspond precisely to individual grain tissues, but the outer fractions (1 and 2)

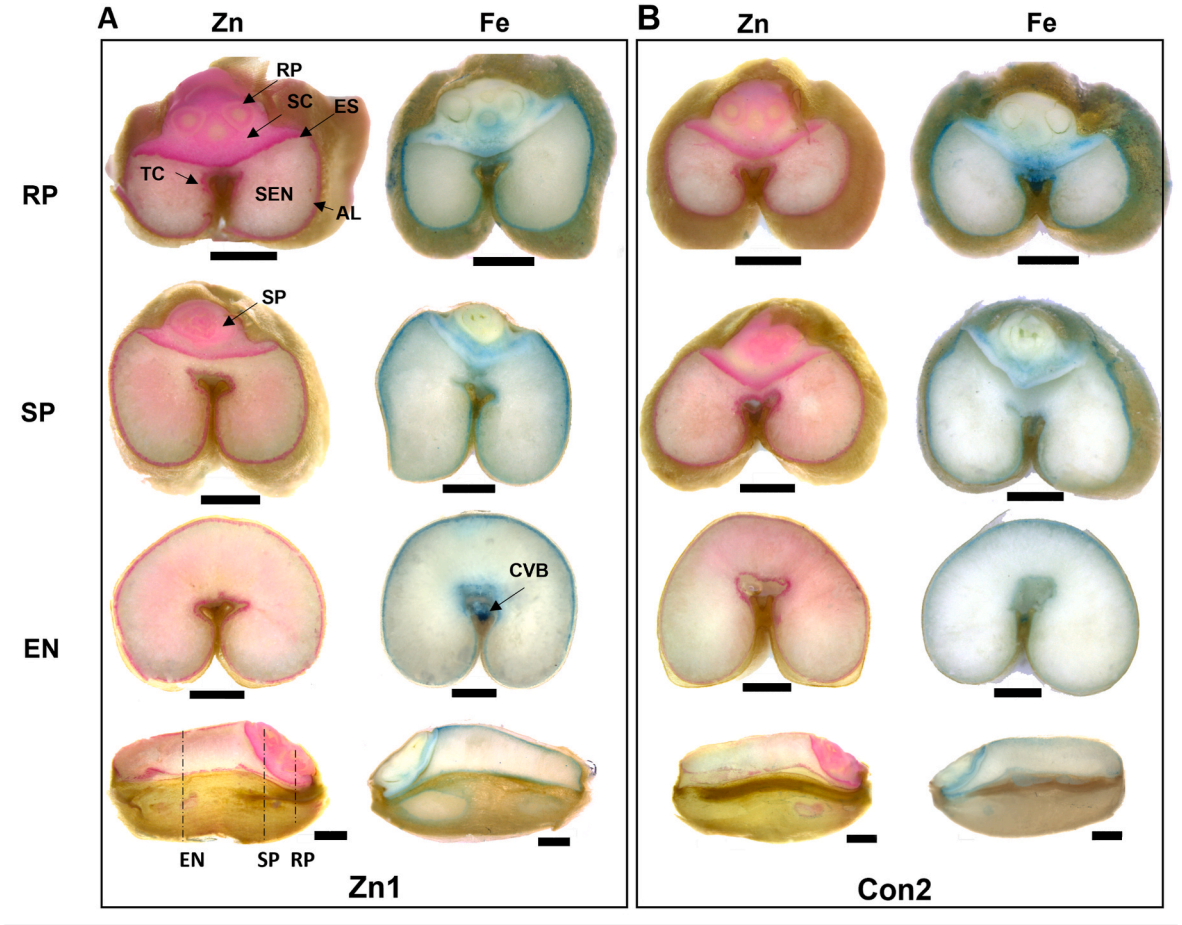

Fig. 2. Localisation of Zn and Fe by dithizone staining and Prussian blue staining of mature grain of Zn1 (A) and Con2 (B). RP, root primordium; SP, shoot primordium; EN, endosperm; SEN, starchy endosperm; SC, scutellum; ES, epithelium of scutellum; AL, aleurone layer; TC, transfer cell; CVB, crease vascular bundle. Scale bars represent 1000 μM. (For interpretation of the references to colour in this figure legend, the reader is referred to the Web version of this article.)

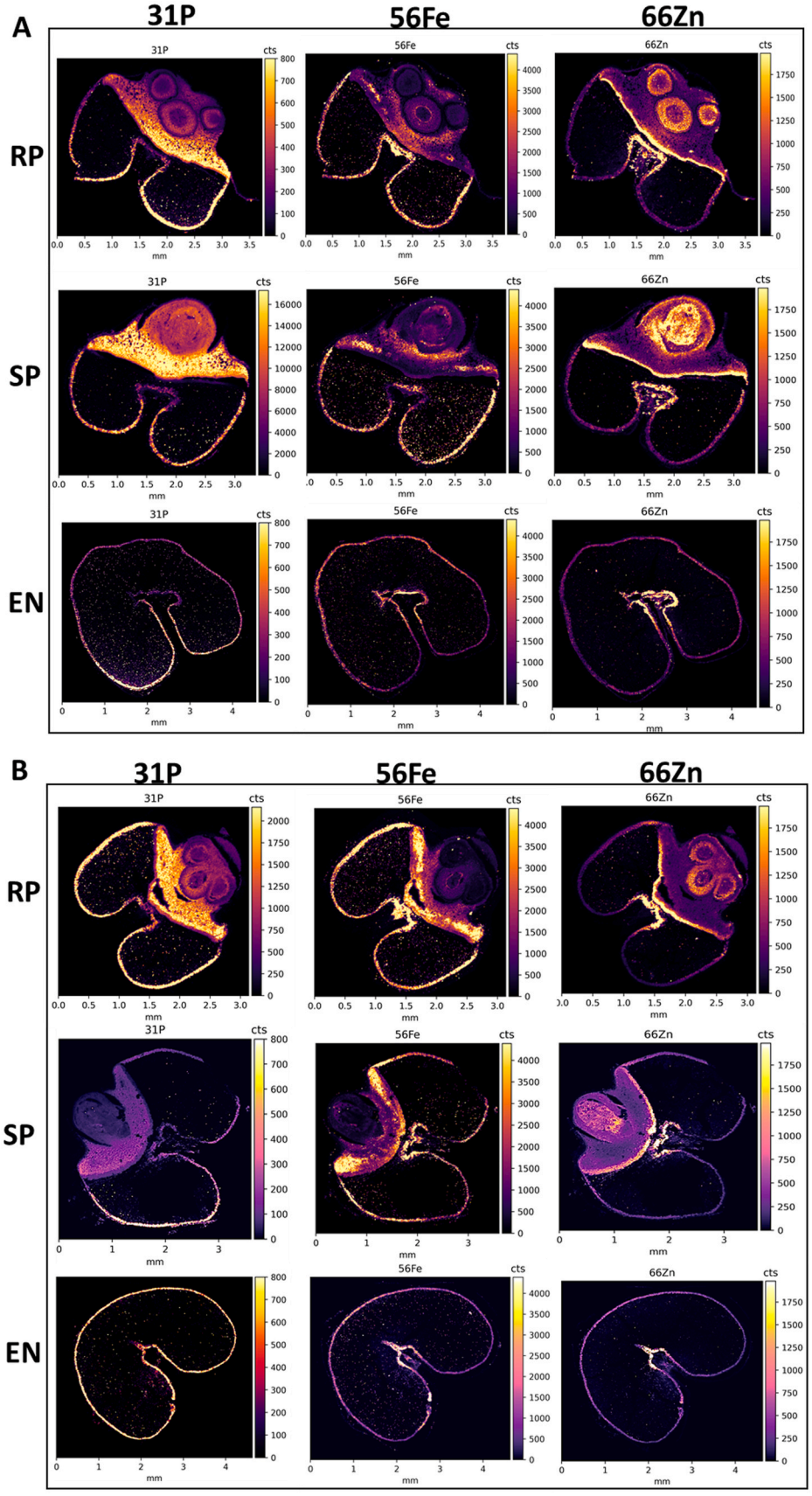

Fig. 3. Localisation of P, Fe and Zn in Zn1 (A) and Con2 (B) by LA-ICP-MS. RP, transverse section through root primordium of embryo; SP, section through shoot primordium of embryo; EN, section through endosperm distal to embryo. cts represents the counts of each element.

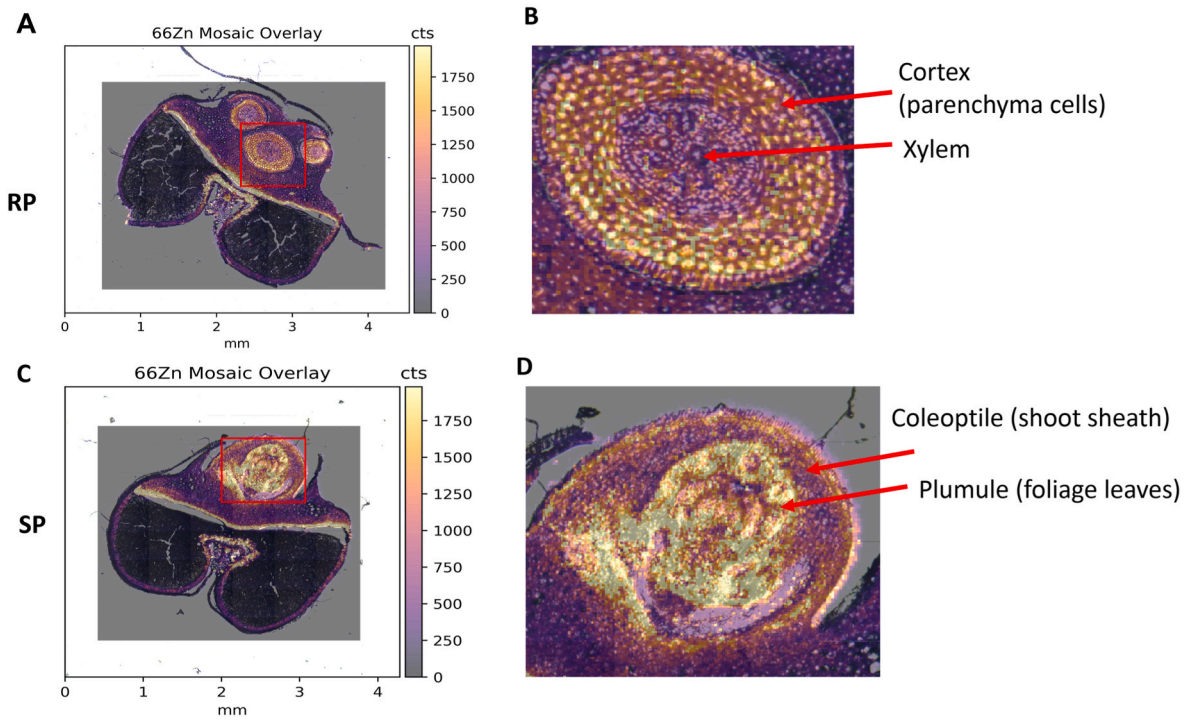

Fig. 4. Localisation of Zn in transverse sections of mature grain of Zn1 by LA-ICP-MS merged with bright field. A, section through the root primordium (RP) of embryo; B, section through the shoot primordium (SP) of embryo; C and D, enlargements of areas shown by red boxes in A and B, respectively. (For interpretation of the references to colour in this figure legend, the reader is referred to the Web version of this article.)

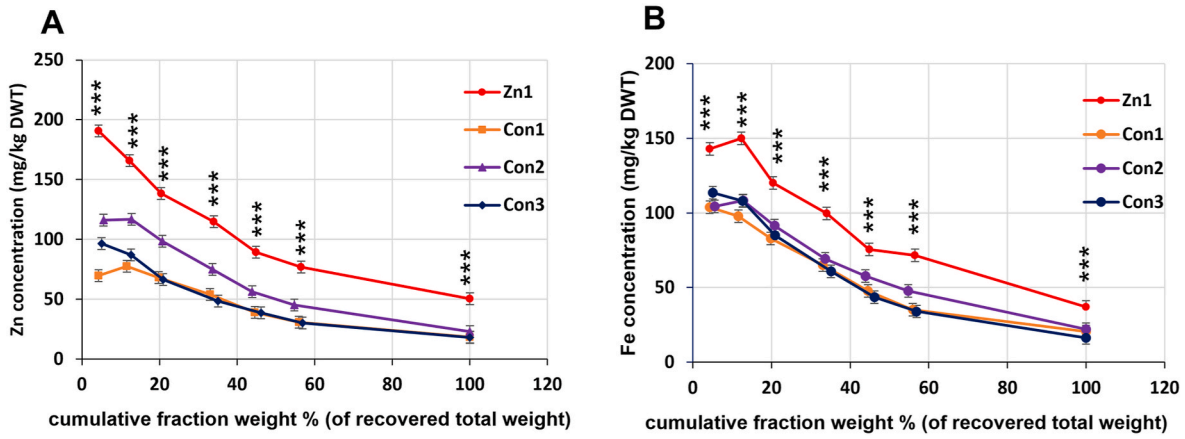

Fig. 5. Concentrations of Zn (A) and Fe (B) in pearling factions of grains of the four wheat lines grown in 2019. The six fractions accounted cumulatively for 4% (mainly embryo and bran, F1), 11% (enriched in aleurone, F2), 18% (enriched in sub-aleurone, F3), 30% (inner starchy endosperm, F4), 40% (inner starchy endosperm, F5), and 50% (inner starchy endosperm, F6) of the total grain weight, and the remaining core for 50% of the total seed weight (central inner endosperm). Error bars shown are standard errors of mean. Asterisks (***) indicated significant differences ($P < 0.001$) between Zn1 and three controls determined by ANOVA. The least significance difference (LSD) values (5%) are 15.24 and 11.91 for Zn and Fe concentrations respectively.

accounting for cumulatively 4% and 11% of total weight, correspond broadly to the bran (outer layers comprising mainly the pericarp, embryo and aleurone), fractions 3 to 6 to the outer part of the starchy endosperm (with fraction 5 being the most central) and the core remaining after pearling to the central starchy endosperm.

ANOVA (Supplementary Table S2) showed statistically significant differences between the distributions of Zn between Zn1 and the average of the control lines ($p < 0.001$) but also differences between the three control lines ($p = 0.012$) (with Con3 differing based on the means and LSD (14.48)). The differences between the concentrations of Zn in Zn1 and the means of the control lines and between the three control lines were also greater for fractions 1 and 2 than for the other fractions. There are also significant differences between the concentrations of Fe in Zn1 and the mean of the control lines ($p < 0.001$) but no evidence of differences between the control lines ($p = 0.103$).

These analyses therefore showed that although the pearling fractions of Zn1 consistently contained higher concentration of both Fe and Zn there were no consistent differences between their distributions between pearling fractions between Zn1 and the control samples.

Micronutrients present in the aleurone layer and scutellum of cereals are mainly chelated to phytic acid to form phytates whereas there is no evidence for the presence of phytates in the starchy endosperm cells. The strong correlations between the concentrations of Fe and Zn in fractions F2 to F6 and the core with the concentration of P (R^2 values above 0.98)

(Supplementary Fig. S2) therefore suggests that the Fe and Zn present in the starchy endosperm fractions (3–6 and the core) were derived from the presence of material from the aleurone which is not completely removed in Fractions 1 and 2 due to the elongated shape of the grain and the presence of the crease. The ratios of P to Fe and Zn were lower in Fraction 1 than in the other fractions which is consistent with the presence of minerals which are not present in phytates in the outer bran layers (notably the pericarp).

3.4. Accumulation of Fe and Zn in developing grain

The time course of accumulation of Fe and Zn in developing caryopses of Zn1 and the three control lines grown in the field in 2018 was determined by analysing three time points: the start of grain filling (16 days post anthesis, DPA), the middle of grain filling (22 DPA) and the end of grain filling (30 DPA). The total concentrations of Fe and Zn were substantially higher in Zn1 throughout development (Fig. 6A) and ANOVA (Supplementary Table S2) showed significant differences between Zn1 and the averages of the control lines ($p < 0.001$ for Zn and Fe) but no evidence of differences between the control lines ($p = 0.542$ for Zn, $p = 0.507$ for Fe). There were also significant differences between the concentrations of Zn and Fe between stages for all lines ($p < 0.001$).

Embryos were prepared by hand dissection at 22 and 30 days (Fig. 6B). The concentration of Zn was clearly higher in Zn1 and ANOVA showed a significant difference between the concentrations in Zn1 and the control lines ($p < 0.001$). However, no significant differences were observed in the concentrations of Fe between Zn1 and the three control lines.

The developing caryopses (after removal of the embryos) were also divided into three approximately equal parts corresponding to the proximal (embryo) part (end1), central part (end2) and distal part (end3) (Fig. 6C and D). Both minerals were enriched in the proximal part (end1) and low in the central (end2) and distal (end3) parts with Zn and Fe being higher in Zn1 than in the control lines. ANOVA showed differences in the concentrations of Zn and Fe between Zn1 and the mean of the control lines ($p < 0.001$) but not between the control lines themselves ($p = 0.208$ for Zn, $p = 0.223$ for Fe). The concentrations of Zn and Fe were also significantly enriched in the distal (end1) sections of Zn compared to the controls at all stages of development (Zn, $p < 0.001$, LSD = 0.13981; Fe, $p < 0.001$, LSD = 0.17070) (Supplementary Table S2). There was also a significant effect of stage ($p < 0.001$) and an interaction of stage with linetype ($p < 0.001$) with the differences in both Zn and Fe between Zn1 and controls increasing with stage.

Finally, the distributions of Fe and Zn in developing caryopses of Zn1 and Con2 were determined by histochemical staining of transverse and longitudinal sections of grain grown in the glasshouse (Supplementary Fig. S3). This showed that the distributions of the minerals at 21 DPA (mid-grain filling) and 28 DPA (late grain filling) were essentially the same as those determined in the mature grains (Fig. 2), showing that the minerals were not redistributed within the caryopses during the middle and late stages of grain development.

4. Discussion

Although wheat is a major contributor to dietary intake of Fe and Zn, their contributions are limited by two factors: the concentrations of the

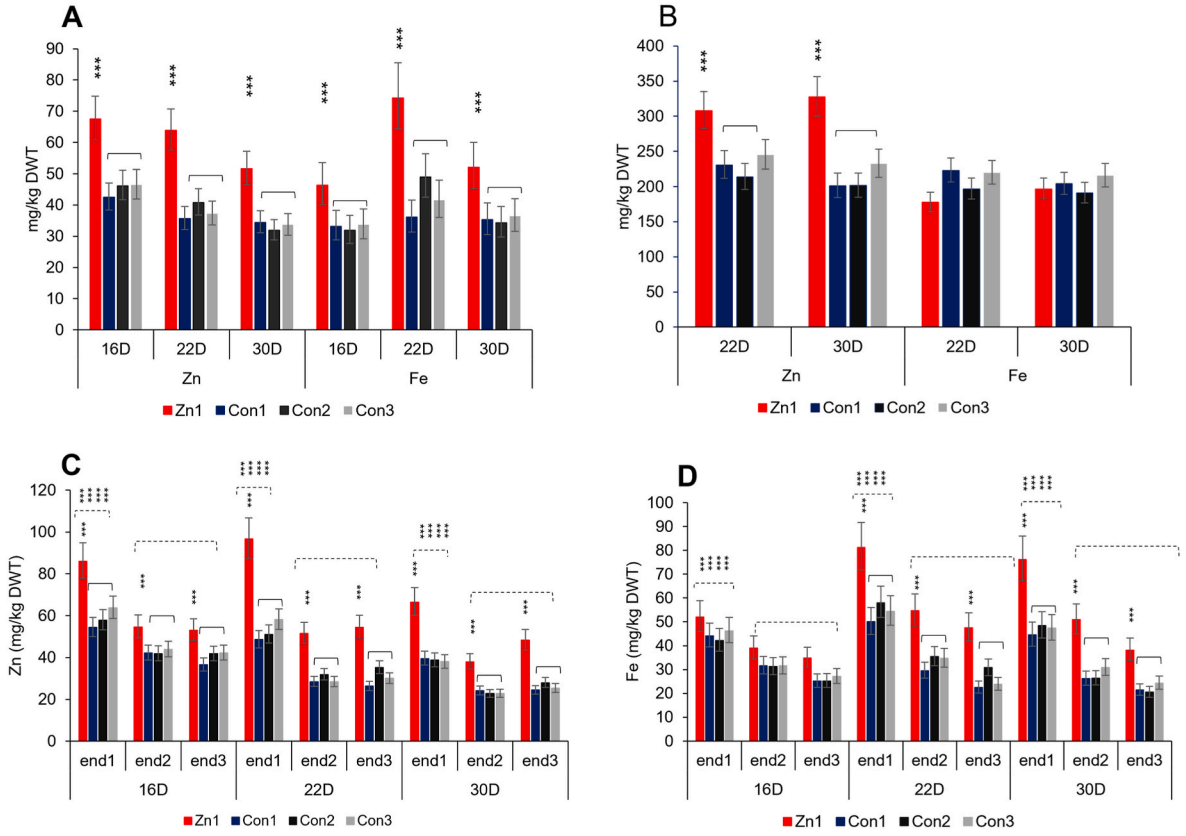

Fig. 6. The concentrations of Zn and Fe in developing whole caryopses, embryos and longitudinal segments of caryopses grown in the field in 2018. (A). Whole caryopses. The concentrations of Fe and Zn are significantly higher in Zn1 at three development stages ($P < 0.001$). (B). Embryos. The Zn concentrations are significantly higher in Zn1 than in the three control lines at 22 and 30 DPA ($P < 0.001$). (C) Zn and (D) Fe in segments of caryopses after removal of embryos. end1, proximal segment; end2, middle segment; end3, distal segment. Significantly higher concentrations of Zn and Fe are present in the proximal segments (end1) of the four lines than in the other segments (end2 and end3) ($P < 0.001$) and in the three segments of Zn1 than the three control lines (with the exception of Fe at 16 DPA). Asterisks (***) indicated the significant differences ($P < 0.001$) between Zn1 and three controls detected by ANOVA. Error bars represent confident intervals (95%).

minerals in the grain and their bioavailability. Velu et al. (2018) reported the development of novel wheat lines containing higher levels of Zn in the grain, by exploiting natural variation in concentration (genetic biofortification). We have confirmed the high Zn status of one of these lines grown in field trials in the UK, showing increases in Zn concentration (mg/g dry wt) of 77.14% and 80.67% compared to the means of three control lines in 2018 and 2019, respectively. Furthermore, the biofortified line also contained higher concentrations of Fe in both years (by 48.31% and 50.01% relative to the control lines). Since the lines studied are not adapted to the UK climate, the presence of high minerals indicates that the trait is robust across environments.

The bioavailability of Fe and Zn in wheat is limited by their location and form. Both minerals are concentrated in the aleurone layer and in the embryo, but they differ in their relative distributions between and within these tissues. Iron is more highly concentrated in the aleurone layer and the scutellum (cotyledon) of the embryo, while Zn is less highly concentrated in the aleurone layer and more concentrated in the embryo, where it is present in the embryonic axis (plumule and radicle) as well as the epithelium of the scutellum.

Minerals (including Fe and Zn) in the aleurone layer and scutellum of wheat and other cereals are largely present as salts of phytic acid (inositol hexakisphosphate) (Neal et al., 2013; Persson et al., 2009). Minerals bound to phytate have poor bioavailability because they have low solubility and are not accessible to Fe transporters in the human gastro-intestinal tract due to the lack of specific enzymes that cleave the Fe−phytate complexes (Schlemmer et al., 2009). By contrast, the Zn present in the embryonic axis may be associated with enzymes and other proteins (as it occurs in thousands of plant proteins (Broadley et al., 2007)) and may therefore have higher bioavailability. This difference in distribution and form may account for the higher bioavailability of Zn in wheat, estimated as about 25% compared to 10% for Fe (Bouis et al., 2010).

We therefore compared the distribution of Fe and Zn in grain of the biofortified and control lines of wheat, using a combination of approaches: sequential removal of layers from the grain by pearling, histochemical staining and LA-ICP-MS. This demonstrated that the minerals had identical locations in the biofortified and control lines, suggesting that their relative bioavailability to humans was not affected. This location also means that Fe and Zn are severely depleted in white flour, although the low levels that are present have relatively high bioavailability (Eagling et al., 2014a, 2014b).

Most of the Zn and Fe is localized in the outer layer of the grain and wholegrain wheat flour provides more Zn than highly refined white flour. This supports the strategy of increasing the intake of foods made from wholegrains of Zn-fortified wheat in the CIMMYT target regions of South Asia and Sub-Saharan Africa. However, whole grains also have high contents of phytate which reduces Zn bioavailability. It has been reported that fermentation of wheat dough leads to breakdown of phytate by phytase enzyme and increases the bioavailable Zn and Fe (Rodriguez-Ramiro et al., 2017) and fermentation is widely used to prepare foods in North Africa and West Asia (various types of flatbread), South Asia (naan) and Africa (injura in Ethiopia). Therefore, the consumption of whole grain wheat flour can help ensure optimal intake of Zn in populations with low Zn status.

Milling to remove the bran reduces the Zn concentration of biofortified wheat. However, the consumption of refined flour made from Zn-biofortified wheat can still deliver enough Zn to have a significant impact on the health of populations that rely heavily on wheat if the extraction rate is lowered to include aleurone tissue in the flour. While refined flours have less phytate, they also have less Zn, and consequently, the amount of bioavailable Zn may not differ greatly between whole meal and refined flours.

The concentrations of minerals in the aleurone layer and embryo, as well as their low bioavailability therefore represents a significant limitation for improving the contribution of wheat to the human diet using conventional genetic improvement. However, it is amenable to genetic engineering, by introducing mechanisms to concentrate minerals in the starchy endosperm (white flour).

Minerals enter the grain through the maternal and modified aleurone transfer cells in the crease of the grain and are transported across the starchy endosperm to the embryo and aleurone layer (Sheraz et al., 2021). Hence, strategies have been developed to trap the minerals which are transported and retain them in the starchy endosperm cells. The first strategy to be adopted was to bind minerals in the starchy endosperm cells by over-expression of a gene encoding the enzyme nicotianamine synthase (NAS). This enzyme catalyses the synthesis of nicotianamine (NA), a metal chelator which plays key roles in the chelation and transport of metals, including Fe and Zn, in higher plants (von Wiren et al., 1999). NA is also the precursor for the biosynthesis of 20-deoxymugenic acid (DMA), a phytosiderophore which also chelates Fe and Zn, and there is evidence that these two compounds, NA and DMA, are the main chelators of Fe in white flour of wheat (Eagling et al., 2014a). The strategy was initially applied to rice, where expression of NAS led to 2.2-fold and 2.9-fold increases in the concentrations of Zn and Fe, respectively, with both minerals showing high bioavailability in mice (Lee et al., 2009), and it has since been applied to wheat grain (Zheng et al., 2010; Beasley et al., 2019; Johnson et al., 2011; Singh et al., 2017). The second strategy is to express genes encoding metal transporters to sequester the metals into the vacuoles of the starchy endosperm cells. This has been successfully used for Fe in wheat (Beasley et al., 2019; Singh et al., 2017) and for Zn in barley (Menguer et al., 2018). However, the minerals may not be uniformly distributed within the starchy endosperm. For example, Beasley et al. (2019) showed that whereas Fe was distributed throughout the starchy endosperm, Zn was concentrated in the region surrounding the crease when the rice *OsNAS2* gene was expressed in wheat using a constitutive promoter. Similarly, Connorton et al. (2017) showed that Fe was concentrated in the starchy endosperm surrounding the crease when the HMW subunit promoter was used to drive a wheat vacuolar Fe transporter gene.

The mechanisms determining the increased accumulation of minerals in the biofortified line studied here are not known but could include increases in source activity (increased uptake and/or transport from roots and vegetative tissues), enhanced partitioning between vegetative and grain tissues, increased sink activity (increased demand from the developing grain) or combinations of these processes. Irrespective of this, it would be interesting to combine genetic biofortification with the transgenic approaches discussed above, in order to direct the additional minerals into bioavailable forms throughout the starchy endosperm (reviewed by Balk et al., 2018).

Declaration of interests

The authors have no competing interests.

Acknowledgements

Rothamsted Research receives strategic funding from the Biotechnology and Biological Sciences Research Council (BBSRC) and the work forms part of the Designing Future Wheat strategic programme (BB/P016855/1). LA-ICP-MS work was carried out at the London Metallomics Facility funded by the Wellcome Trust (grant reference 202902/Z/16/Z). The authors thank Andrew Riche and David Steele for management of the field plots and samples and Saroj Parmar for the sample preparation for ICP-OES.

Appendix A. Supplementary data

Supplementary data to this article can be found online at https://doi.org/10.1016/j.jcs.2022.103470.

References

Balk, J., Connorton, J.M., Wan, Y., et al., 2018. Improving wheat as a source of iron and zinc for global nutrition. Nutr. Bull. https://doi.org/10.1111/nbu.12361.

Bates, B., Lennox, A., Prentice, A., et al. (Eds.), 2014. National Diet and Nutrition Survey: Results from Years 1-4 (Combined) of the Rolling Programme (2008/2009 – 2011/2012). Public Health England, London, UK. Executive Summary. https://assets.publishing.service.gov.uk/government/uploads/system/uploads/attachment_data/file/594360/NDNS_Y1_to_4_UK_report_executive_summary_revised_February_2017.pdf.

Bates, B., Lennox, A., Bates, C., Swan, G., et al. (Eds.), 2014. National Diet and Nutrition Survey: Results from Years 1-4 (Combined) of the Rolling Programme (2008/2009 – 2011/2012). Public Health England, London, UK. https://assets.publishing.service.gov.uk/government/uploads/system/uploads/attachment_data/file/594361/NDNS_Y1_to_4_UK_report_full_text_revised_February_2017.pdf.

Beasley, J.T., Bonneau, J.P., Sánchez-Palacios, J.T., et al., 2019. Metabolic engineering of bread wheat improves grain iron concentration and bioavailability. Plant Biotechnol. J. https://doi.org/10.1111/pbi.13074.

Bouis, H.E., Welch, R.M., 2010. Biofortification-a sustainable agricultural strategy for reducing micronutrient malnutrition in the global south. Crop Sci. https://doi.org/10.2135/cropsci2009.09.0531.

Broadley, M.R., White, P.J., Hammond, J.P., et al., 2007. Zinc in plants. New Phytol. https://doi.org/10.1111/j.1469-8137.2007.01996.x.

Connorton, J.M., Jones, E.R., Rodriguez-Ramiro, I., et al., 2017. Wheat vacuolar iron transporter TaVIT2 transports Fe and Mn and is effective for biofortification. Plant Physiol. https://doi.org/10.1104/pp.17.00672.

Eagling, T., Neal, A.L., McGrath, S.P., et al., 2014a. Distribution and speciation of iron and zinc in grain of two wheat genotypes. J. Agric. Food Chem. https://doi.org/10.1021/jf403331p.

Eagling, T., Wawer, A.A., Shewry, P.R., et al., 2014b. Iron bioavailability in two commercial cultivars of wheat: comparison between wholegrain and white flour and the effects of nicotianamine and 2'-deoxymugineic acid on iron uptake into Caco-2 cells. J. Agric. Food Chem. https://doi.org/10.1021/jf5026295.

Johnson, A.A.T., Kyriacou, B., Callahan, D.L., et al., 2011. Constitutive overexpression of the *OsNAS* gene family reveals single-gene strategies for effective iron- and zinc-biofortification of rice endosperm. PLoS One. https://doi.org/10.1371/journal.pone.0024476.

Lee, S., Jeon, U.S., Kim, Y.-K., et al., 2009. Iron fortification of rice seeds through activation of the *nicotianamine synthase* gene. PNAS USA. https://doi.org/10.1073/pnas.0910950106.

Lowe, N.M., Zaman, M., Moran, V.H., et al., 2020. Biofortification of wheat with zinc for eliminating deficiency in Pakistan: study protocol for a cluster-randomised, double-blind, controlled effectiveness study (BIFIFED2). BMJ Open. https://doi.org/10.1136/bmjopen-2020-039231.

Menguer, P.K., Vincent, T., Miller, A.J., et al., 2018. Improving zinc accumulation in cereal endosperm using HvMTP1, a transition metal transporter. Plant Biotechnol. J. https://doi.org/10.1111/pbi.12749.

Neal, A.L., Geraki, K., Borg, S., et al., 2013. Iron and zinc complexation in wild-type and ferritin-expressing wheat grain: implications for mineral transport into developing grain. J. Bioinorg. Chem. https://doi:10.1007/s00775-013-1000-x.

Persson, D.P., Hansen, T.H., Laursen, K.H., et al., 2009. Simultaneous iron, zinc, sulfur and phosphorus speciation analysis of barley grain tissues using SEC-ICP-MS and IP-ICP-MS. Metallomics. https://doi.org/10.1039/b905688b.

Rathan, N.D., Sehgal, D., Thiyagarajan, K., et al., 2021. Identification of genetic loci and candidate genes related to grain zinc and iron concentration using a zinc-enriched wheat 'zinc-shakti. Front. Genet. https://doi.org/10.3389/fgene.2021.652653.

Rodriguez-Ramiro, I., Brearley, C.A., Bruggaber, S.F.A., et al., 2017. Assessment of iron bioavailability from different bread making processes using an *in vitro* intestinal cell model. Food Chem. https://doi.org/10.1016/j.foodchem.2017.01.130.

SACN, 2010. Iron and Health. TSO (The Stationary Office), London, UK. https://assets.publishing.service.gov.uk/government/uploads/system/uploads/attachment_data/file/339309/SACN_Iron_and_Health_Report.pdf.

Schlemmer, U., Frølich, W., Prieto, R.M., et al., 2009. Phytate in foods and significance for humans: food sources, intake, processing, bioavailability, protective role and analysis. Mol. Nutr. Food Res. https://doi.org/10.1002/mnfr.200900099.

Sheraz, S., Wan, Y., Venter, E., et al., 2021. Subcellular dynamic studies of iron reveal how tissue-specific distribution patterns are established in developing grain. New Phytol. https://doi.org/10.1111/nph.17440.

Shi, Z., Wang, Y., Wan, Y., et al., 2019. Gradients of gluten proteins and free amino acids along the longitudinal axis of developing caryopses of bread wheat. J. Agric. Food Chem. https://doi.org/10.1021/acs.jafc.9b02728.

Singh, S.P., Keller, B., Gruissem, W., et al., 2017. Rice *NICOTIANAMINE SYNTHASE 2* expression improves dietary iron and zinc levels in wheat. Theor. Appl. Genet. https://doi.org/10.1007/s00122-016-2808-x.

Tosi, P., Sanchis Gritsch, C., He, J., et al., 2011. Distribution of gluten proteins in bread wheat (*Triticum aestivum*) grain. Ann. Bot. https://doi:10.1093/aob/mcr098.

Velu, G., Singh, R.P., Crespo-Herrera, L., et al., 2018. Genetic dissection of grain zinc concentration in spring wheat for mainstreaming biofortification in CIMMYT wheat breeding. Sci. Rep. https://www.nature.com/articles/s41598-018-31951-z.

von Wiren, N., Klair, S., Bansal, S., et al., 1999. Nicotianamine chelates both Fe^{III} and Fe^{II}. Implications for metal transport in plants. Plant Physiol. https://doi.org/10.1104/pp.119.3.1107.

VSN International, 2020. In: Genstat for Window 21st Edition. VSN International, Hemel Hempstead, UK. Web page: Genstat.co.uk.

WHO, 2013. World Health Report: Research for Universal Health Coverage. World Health Organization, Geneva, Switzerland. https://www.who.int/whr/2013/report/en/.

WHO, 2015. The Global Prevalence of Anaemia in 2011. World Health Organization, Geneva, Switzerland. https://www.who.int/nutrition/publications/micronutrients/global_prevalence_anaemia_2011/en/.

Zhao, F.J., Su, Y.H., Dunham, S.J., et al., 2009. Variation in mineral micronutrient concentrations in grain of wheat lines of diverse origin. J. Cereal. Sci. https://doi.org/10.1016/j.jcs.2008.11.007.

Zheng, L., Cheng, Z., Ai, C., et al., 2010. Nicotianamine, a novel enhancer of rice iron bioavailability to humans. PLoS One. https://doi.org/10.1371/journal.pone.0010190.